

Monitoring of LHAASO-WCDA Performance by Using Crab Nebula and Moon Shadow Observations

Xiaoyu Wang,^a Cuandong Gao,^b Yanjin Wang,^c Min Zha,^{d,e} Xinhua Ma^{d,e} and Shuwang Cui^{a,*} for the LHAASO collaboration

^aHebei Normal University, 050024, Shijiazhuang, China

^bShandong University, 266237, Qingdao, China

^cCollege of Sciences, Northeastern University, 110819 Shenyang, Liaoning, China

^dKey Laboratory of Particle Astrophysics, Institute of High Energy Physics, Chinese Academy of Sciences, Beijing 100049, China

^eTIANFU Cosmic Ray Research Center, Chengdu, Sichuan 610000, China

E-mail: cuisw@hebtu.edu.cn

The Water Cherenkov Detector Array (WCDA), the center array of the Large High Altitude Air Shower Observatory (LHAASO), is highly sensitive to VHE gamma-ray sources and dedicated to survey the northern sky in the energy range from 100 GeV to 30 TeV. A monthly analysis of Crab nebular gamma ray source and the moon shadow were performed. The results about angular resolution and the pointing error of WCDA is presented. Besides the west-shifted position of the moon shadow is also presented in this work.

38th International Cosmic Ray Conference (ICRC2023)
Jul 26–Aug 3, July,2023
Nagoya, Japan



*Speaker

1. Introduction

The LHAASO [1] is located at Mt. Haizi (4410 m a.s.l., 600 g/cm²) in Daocheng, Sichuan province, P.R. China. LHAASO consists of 1.3 km² array (KM2A) of electromagnetic particle detectors (ED) and muon detectors (MD), a water Cherenkov detector array (WCDA) [2] with a total active area of 78,000 m², 18 wide field-of-view air Cherenkov telescopes (WFCTA). Civil construction of LHAASO started in the middle of 2016 and the whole array was completed in July of 2021. LHAASO takes the function of hybrid technology to detect cosmic rays and to upgrade greatly the resolving power between gamma rays and cosmic rays. The LHAASO makes the full-sky survey to find new gamma ray sources, to obtain the highest sensitivity of gamma ray detection at the high energy band of greater than 30 TeV, and to make the very high precision measurement on the component energy spectra of cosmic rays in a broad energy range of 5 orders of magnitude, in order to provide the evidence for revealing the mystery of the origin of cosmic ray. The main working energy range of WCDA is from 0.1 TeV to 50 TeV, which is the energy range of cosmic rays that it can detect. WCDA is a water Cherenkov detector that measures the Cherenkov light produced when cosmic rays interact with water molecules to determine the energy and direction of cosmic rays. With high detection efficiency and energy resolution in the energy range from 0.1 TeV to 50 TeV, WCDA can provide important data for the study of cosmic rays.

The Crab Nebula, serving as a young and intense supernova remnant, is a crucial celestial object in cosmic ray research. It has been extensively studied through its spectrum and is a very bright and stable high-energy radiation source, taken as a standard candle in multiple wavelength bands. Its significance, location, and angular resolution can be utilized to monitor the stability of the detector. The moon shadow is a significant astronomical phenomenon that occurs when primary cosmic rays are blocked by the moon and deviated by planetary magnetic field during propagation towards the Earth. the moon shadow can be utilized to calibrate detector energy scales. By keeping on observing the Crab Nebula and the moon shadow, the stability of the WCDA detector can be monitored to guarantee the accuracy and dependability of EAS measurements. Long-term stability can be evaluated by comparing observation results at different time periods.

2. WCDA Detectors

WCDA is a ground-based air-shower detector array based on water cherenkov technique conceived for investigating steady and transient VHE gamma-ray sources located at the northern sky from 0.1 TeV to 30 TeV. WCDA spans an area of 78,000 m² and is composed of three water ponds, partitioned into 3120 detector cells (Figure 1 left panel). WCDA-1 and WCDA-2 have an area of 150 m × 150 m, and WCDA-3 has an area of 300 m × 110 m, with an effective water depth of 4 m. Each cell contains a large photomultiplier tube (PMT) and a small PMT with the photocathode facing upward, which is utilized to detect Cherenkov photons produced by secondary particles in cosmic ray showers within the water. There is an upward-looking 8 inch photomultiplier tube (PMT) and 1.5 inch PMT in each cell of WCDA-1, while a 20 inch PMT and 3 inch PMT are hung in each cell of WCDA-2 and WCDA-3. As one example, one triggered event is shown in Figure 1 right panel.

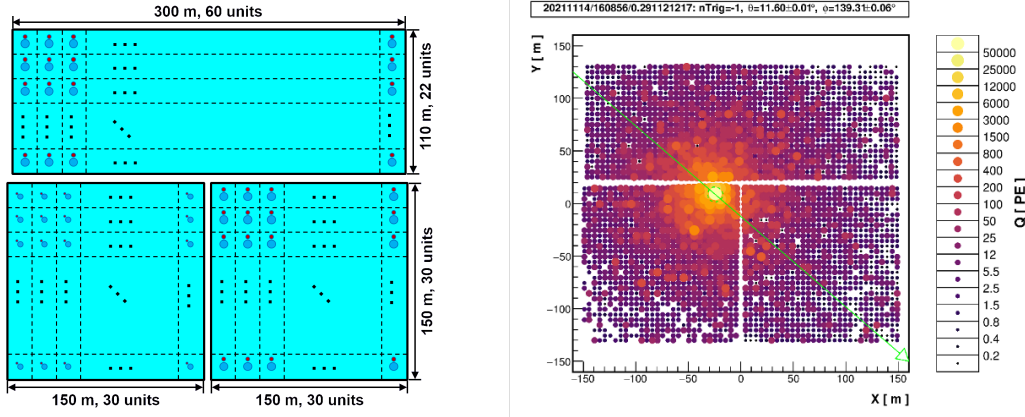


Figure 1: Schema of the WCDA layout(left panel) and a read event,a real event recorded by WCDA detector on 14th Nov.2021 (right panel) .The color code in the right figure corresponds to the charge in photo-electron (PE),while the green arrows indicate the reconstructed direction.

3. Detail

3.1 Significance estimation

The equal-zenith angle method is used in this paper for significance estimation. Four background source windows are symmetrically distributed on either side of the forward source window, with an angular distance of 5° between each edge, and a maximum zenith angle of less than 50° . Due to the limited range of the zenith angle, the minimum zenith angle is greater than 8.53° . Significance is calculated using the Li-Ma[3] formula:

$$S = \frac{N_{on} - \alpha N_{off}}{\sqrt{N_{on} + \alpha^2 N_{off}}} \quad (1)$$

3.2 Data selections

We use only events with zenith angles less than 50° in this analysis, corresponding to the survey region in the declination band from -20° to 80° . For the WCDA data, events are divided into five groups according to the number of hits (Nhit),i.e., 100-200, 200-300, 300-500, 500-800, ≥ 800 . For Crab-like sources, the corresponding energies roughly range from 1 TeV to 25 TeV[4].

This paper presents the monitoring results of the WCDA probe during its 10-month operation from January 2022 to December 2022. Significance analysis is conducted separately for each month, with a pinness < 1.1 cut applied to the Crab. The significance of the Crab and Moon observations was analyzed for each month with the condition of $N_{hit} > 100$. ("Pinness"[5] refers to the precision of the particle hit position at the center of the detector. The WCDA detector is composed of many small detection units, each of which has a (photomultiplier tube) PMT and some scintillators. When a particle passes through a scintillator, the scintillator emits photons, and the PMT measures the signals of these photons. By measuring the signals from different scintillators, the hit position of the particle can be determined. Pinness refers to the accuracy of this position, that is, the ability to determine the hit position.)

4. Results for Crab nebula and moon shadow

4.1 Crab nebula

After selecting data under the aforementioned conditions, data from March 1, 2021 to December 31, 2021 were used for Crab significance analysis, resulting in a significance of 193.98σ for Crab under $N_{hit} > 100$. Subsequently, we analyzed the monthly significance of Crab under the condition of $N_{hit} > 100$, and Figure 2 displays the corresponding 2D distribution of significance for Crab. It is evident that the shape and position of Crab for each month do not exhibit any significant anomalies, which is in line with our expectations.

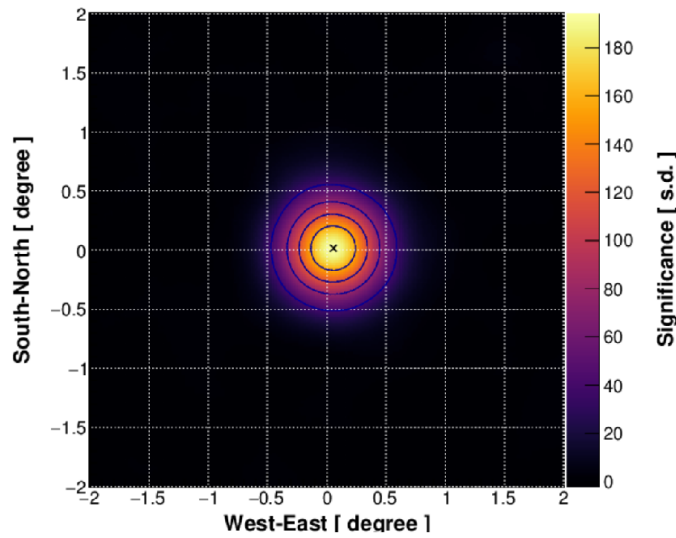


Figure 2: This is a 2-dimensional significance map centered on the position of the Crab Nebula, covering the period from March 1, 2021 to December 31, 2021. It shows a 10-month map of the significance of the Crab Nebula under the condition of $N_{hit} > 100$.

From Figure 3, it can be observed that the position of the Crab center in the Dec direction is 21.09° and in the RA direction is 83.64° , and the results for each month are consistent within the error range.

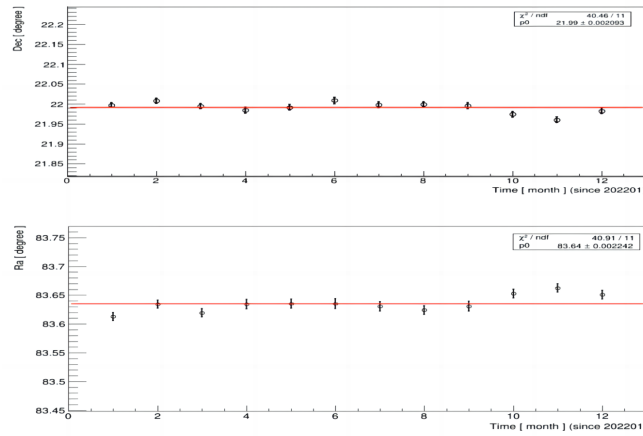


Figure 3: The monthly offsets of the Crab center in the RA direction (shown in the lower image) and the Dec direction (shown in the upper image) for $N_{\text{hit}} > 100$.

4.2 Moon shadow results

In this work, a circular window with a radius of 5° around the center of the moon was chosen as the source window, while four equally sized circular windows located on an equatorial band were selected as the background windows. The non-coincidence condition of small zenith angles was used to calculate that the zenith angle of the moon should be greater than 8.5° , which was also used as a minimum threshold for the analysis.

Following the selection of data based on the aforementioned conditions, an analysis of the moon shadow was conducted using data collected from May 1, 2019 to February 29, 2020. The total significance of moon shadow loss for $N_{\text{hit}} > 100$ was 99.8σ .

Long-term observations of moon shadow can serve as a means to test the stability of detector operation and data reconstruction, providing assurance for subsequent physical analyses. The significance of moon shadow for each month under the condition of $N_{\text{hit}} > 100$ was analyzed, and Figure 6 illustrates the corresponding two-dimensional significance distribution of moon shadow significance.

Figure 4 presents the temporal variation of moon shadow significance, which can be visually observed. It is apparent that there were no significant anomalies in the shape and position of the moon shadow for each month, and no anomalies were observed beyond 1.5° from the center of the moon shadow. The positive anomalies did not exceed 3σ , which is consistent with the expected results.

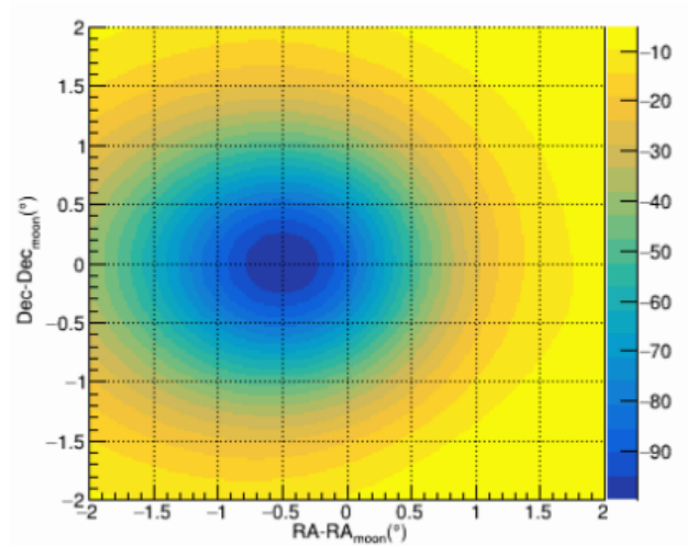


Figure 4: This is a 2-dimensional significance map centered on the position of the moon shadow, covering the period from May 1, 2021 to February 29, 2022. It shows a 10-month map of the significance of the moon shadow under the condition of $N_{hit} > 100$.

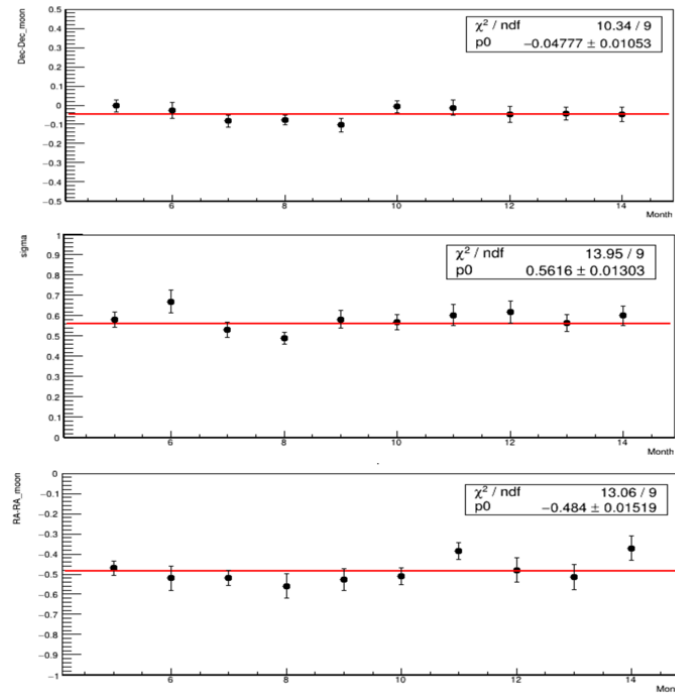


Figure 5: For $N_{hit} > 100$, the offset of the moon shadow center in the RA direction (bottom panel) and the Dec direction (top panel), as well as the Gaussian width of the moon shadow one-dimensional projection in the Dec direction (middle panel) are presented for each month.

Subsequently, we analyzed the position and width of the moon shadow for each month to investigate the long-term stability of the detector (Figure 5). After fitting, the average offset of the

moon shadow center in the Dec direction was found to be -0.047° , with the results for each month being consistent within the error range. The average width of the moon shadow in the Dec direction was 0.56° .

The average offset of the moon shadow center in the RA direction was found to be -0.48° , with the results for each month being consistent within the error range. The absolute value of the moon shadow offset in the RA direction exhibited a positive correlation with the angular resolution, which further reflects the energy threshold. Specifically, larger offsets and angular resolutions indicate a lower energy threshold, while smaller offsets and angular resolutions indicate a higher energy threshold.

The analysis revealed that the energy threshold remained relatively consistent for each month. In summary, the results of the moon shadow position and angular resolution for each month remained consistent, indicating that the detector operated in a stable manner throughout the aforementioned period.

5. Summary

Our detector was very stable from March 2021 to December 31, 2022. We used a reliable method to detect the stability of the detector and plan to use the same method in the future to verify the stability of the detector during other time periods. These results indicate that our detector is reliable and we can trust our experimental results.

6. Acknowledgement

The authors would like to thank all staff members who work at the LHAASO site all year around to keep the system running efficiently and smoothly, even in the demanding conditions at a mean altitude of 4400 meters above sea level. We are grateful to the Chengdu Management Committee of Tianfu New Area for the constant financial support to the research with LHAASO data. This research work is also supported by the National Key R& D program of China, with the grant 2018YFA0404201, 2018YFA0404202 and 2018YFA0404203, the National Natural Science Foundation of China, with NSFC grants 11635011, 11761141001, 11905240, 11503021, 11205126, 11947404, 11675187, U1831208, Schools of Science and Technology Plan from SiChuan Province grant No.20SYSX0294, and Thailand Science Research and Innovation grant RTA6280002.

References

- [1] X. Ma, *et al.*, Chapter 1 LHAASO instruments and detector technology. Chinese Physics, C 46 (2022) 030001.
- [2] J. Y. Liu, B. Gao, C. X. Yu, M. J. Chen, Y. A. Luo, Z. G. Yao, M. Zha, H. R. Wu, H. C. Li and X. J. Wang, JINST **12**, no.10, P10021 (2017) doi:10.1088/1748-0221/12/10/P10021
- [3] T. P. Li and Y. Q. Ma, Astrophys. J. **272** (1983), 317-324 doi:10.1086/161295
- [4] Z. Cao *et al.* [LHAASO], [arXiv:2305.17030 [astro-ph.HE]].

- [5] A. U. Abeysekara *et al.* [HAWC], Phys. Rev. D **97**, no.10, 102005 (2018)
doi:10.1103/PhysRevD.97.102005 [arXiv:1802.08913 [astro-ph.HE]].